A Comparison of Modeled Drought Conditions from ScenarioMIP Simulations in the Central and Western United States

Dylan Jones

April 6, 2023

Abstract

Using simulation outputs from the Scenario Model Intercomparison Project (ScenarioMIP), we have calculated potential evapotranspiration values using the Penman-Monteith method for four different model outputs. Leveraging the climatic water balance input and the multi-scalar nature of the Standardized Precipitation Evapotranspiration Index, we have calculated drought indices across 30-year climatologies that bookend the 85 year prediction range of the simulations, producing robust datasets. Comparing model performance with respect to their output resolution as well as their Equilibrium Climate Sensitivity, we confirm the findings of the latest IPCC report, predicting increasing drought conditions in the western United States. Despite this general drying predicted in the western United States, our results show a notable wetting trend in the New Mexico-Colorado region, leading to potential questions about the future of the North American Monsoon. While we were unable to make progress in the difficult problem that remains regarding the hydroclimatological future of the American Midwest, we suggest from our results that future ScenarioMIP studies enhance model output resolution.

Introduction

As global temperatures continue to rise as a result of human greenhouse gas emission (Pörtner et al., 2022), humanity faces an increasingly hostile habitat with growing threats of infectious disease (McMichael et al., 2006; Patz et al., 1996), extreme weather (Knutson et al., 2010), and rising sea levels (IPCC, 2022). Another potential hazard with potentially widespread detrimental effects is drought, with the ability to reduce agricultural production (Basara et al., 2013; Vicente-Serrano et al., 2012), increase wildfires (Stevens-Rumann et al., 2018), threaten drinking water supply (Pasteris et al., 2005), and even decrease electricity supply to regions dependent on hydroelectric power (Wan et al., 2021).

While droughts appear a straightforward concept, a variety of metrics exist attempting to accurately quantify persistent soil moisture deficiencies with potentially massive signal discrepancies (Cook et al., 2014; Panu and Sharma, 2002). Also unintuitively, future droughts are likely driven by increases in evaporation-transpiration (ET) rates that outweigh simultaneous precipitation increases, so it is critical to include drought indices that incorporate ET input (Cook et al., 2014). Many regions, such as the western and central United States, show high uncertainty in projected hydroclimatological changes and potentially bear high vulnerability for food, water, and economic security for many in the U.S. and around the world (Basara et al., 2013; IPCC, 2022). Clearly there is a necessity for more research into this field.

This study will use the Standardized Precipitation Evapotranspiration

Index (SPEI; Beguería et al., 2014; Vicente-Serrano et al., 2010), an evolution of the Standardized Precipitation Index (SPI) incorporating climatic water balance (CWB in Eq. 1) as opposed to precipitation alone in its calculation. This important improvement should facilitate more accurate representation of drought conditions in a warming climate that will experience simultaneously increasing precipitation (P; Prein et al., 2017) and potential evapotranspiration (PET; Pan et al., 2015).

$$CWB = P - PET \tag{1}$$

Pulling from four different Scenario Model Intercomparison Project (ScenarioMIP; O'Neill et al., 2016) model simulations, this study will compare and contrast the first (2015-2044) and last (2071-2100) 30-year climatologies of each model to better understand the future of drought in the central and western United States, regions most susceptible to the socioeconomic issues mentioned earlier.

Methods

Data Accumulation and Pre-Processing

ScenarioMIP datasets were downloaded and parsed primarily from the National Center for Atmospheric Research's GLADE storage system with any missing datasets being substituted in from Lawrence Livermore National Laboratory's data request portal (https://esgf-node.llnl.gov/search/cmip6/; Shiogama et al., 2019; Swart et al., 2019; Xin et al., 2019; Yukimoto et al.,

2019). All ScenarioMIP datasets used in this study are forced according to the SSP2-4.5 pathway, an updated version of the RCP4.5 pathway from the preceding CMIP5 experiments. This pathway is designed to represent a moderate warming scenario in which model forcing parameters stabilize at 4.5 $\mathrm{W\,m^{-2}}$, as countries across the globe slowly, but gradually make necessary adaptations to mitigate greenhouse gas emissions (O'Neill et al., 2016; O'Neill et al., 2017).

Models used in this study are required to output 6 monthly-averaged variables: minimum temperature (`tasmin`), maximum temperature (`tasmax`), cloud cover percentage (`clt`), surface pressure (`ps`), surface wind speed (`sfcWind`), and precipitation (`pr`), and all models are members of the r1i1p1f1 ensemble, following the methods of Ruhe, 2022. The four models presented in this study (shown in Table 1) were selected with a preference for higher spatial resolution, the accessibility of their data, and variability of equilibrium climate sensitivity (ECS), a metric calculated by doubling the CO_2 concentration of a given model and measuring surface air temperature difference. This has proven to be a useful way of understanding a given model's response strength to CO_2 forcing, and this study will work to analyze these datasets with this concept in mind.

Following initial dataset accumulation and to ease processing workload of future calculations, all datasets were cropped temporally into files representing the first (2015-2044) and last (2071-2100) 30 years of ScenarioMIP simulations and were also spatially cropped to frame the continental United States. These edits were performed using NCO, a package of shell commands designed to manipulate NetCDF files.

Model Name	Spatial Resolution	ECS
BCC-CSM2-MR (BCC)	**160 × 320**	3.02
CanESM5 (CAN)	64 × 128	**5.64**
MIROC6 (MIROC)	128 × 256	**2.60**
MRI-ESM2-0 (MRI)	**160 × 320**	3.13

Table 1: Four selected models with associated global spatial resolution and ECS computed in Zelinka et al., 2020. Bold fonts denote preferred values, indicating why each model was chosen.

Calculating Potential Evapotranspiration and SPEI

While precipitation is an essential and common output of CMIP6 simulations, PET or latent heat flux, is often omitted from these outputs. To resolve this gap, we will leverage the Penman-Monteith equation (Eq. 2; Allen et al., 1998; Pereira et al., 2015), a powerful PET calculation that includes not only surface temperatures, as other simpler PET calculations such as the Thornthwaite method (Chen et al., 2005), but net surface radiation (R_n), surface wind speed (u_2), and humidity, among others, shown in Eq. 2. This increased complexity results in a more accurate PET estimation, so long as variables relating to incoming solar radiation are available (Sentelhas et al., 2010).

These calculations were completed using the `penman()` function in the R "SPEI" package, using each model's `tasmin`, `tasmax`, `clt`, `ps`, `sfcWind` values as inputs, as well as each grid cell's latitude (as a component of R_n) to

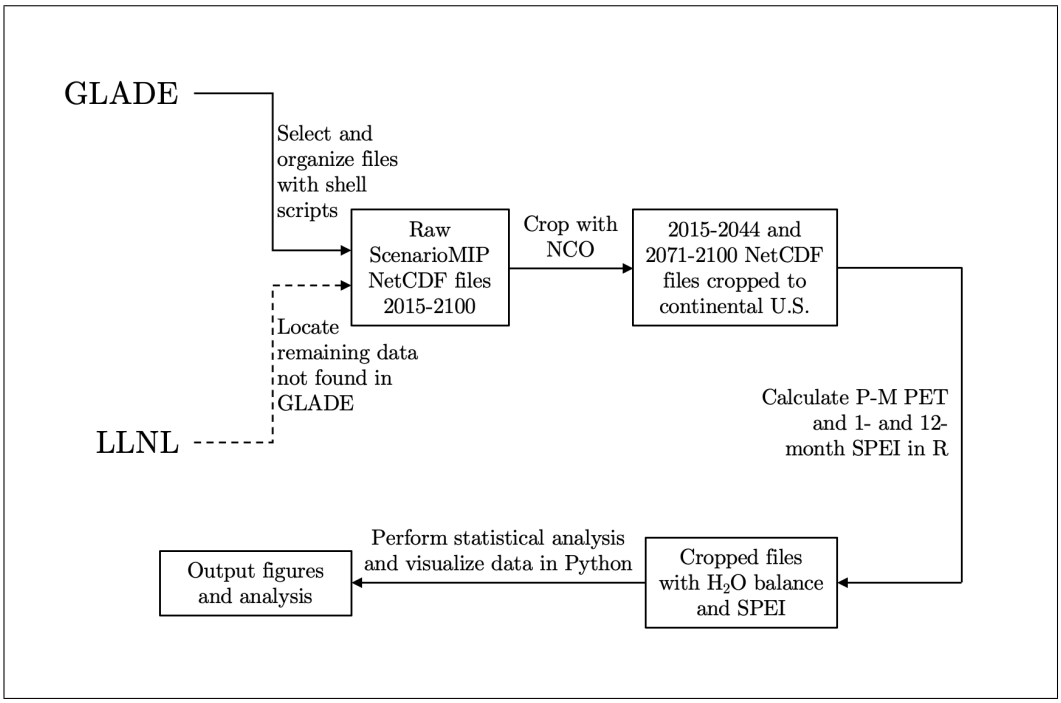

Figure 1: Flowchart depicting data collection, cropping, calculation, and figure output. Dotted lines depict potentially necessary alternate steps.

calculate each grid cells associated PET value. Water balance was calculated after, in accordance with Equation 1.

1- and 12-month SPEI calculations were then completed for all grid cells in each of the four models using the "SPEI" package and the CWB as the only input. SPEI is a relatively straightforward calculation that is entirely-statistically based, having no other climate factors directly impacting the computation. The function simply aggregates each CWB time series value into bins based on the number of months over which the index is being calculated and then the aggregated values are modeled to one of four probability distribution curves. We elected to use the Log-logistic distribution as it is the most commonly used and researched distribution for the index (Vicente-

$$PET = \frac{0.408\Delta(R_n - G) + \gamma(C_n/T + 273)u_2(e_s - e_a)}{\Delta + \gamma(1 + C_d u_2)} \tag{2}$$

Where Δ is the slope of the saturation vapor pressure curve, R_n is net incoming solar radiation, G is soil heat flux density, γ is the pyschrometric constant, C_n and C_d are constants that fluctuate with vegetation type, T is the mean temperature, u_2 is the wind speed at 2 m above the land surface, e_s is the saturation vapor pressure and e_a is the actual vapor pressure (Pereira et al., 2015).

Serrano et al., 2010). The data calculated at each cell across each time period is centered at 0 (no drying or wetting), and has a standard deviation of 1, where 1 represents wetting conditions, and -1 represents drying in that cell.

Data Visualization and Analysis

Before drawing conclusions from the generated data, SPEI values were pulled from the SPEI database (SPEIDB), a collection of calculated index values spanning from January 1901 to December 2021 (Vicente-Serrano et al., 2010). The database values are calculated according to the same Penman-Monteith procedure so these values should be comparable and differences can be attributed solely to the variation in input data.

Plots and analysis for this study were completed in Python using a variety of plotting and data organization tools specialized for geographical plotting and NetCDF datasets. All datasets were regridded with a bilinear interpolation method from their original coordinate grid to the highest resolution (160×320) in order to directly compare results between different models and generate four model mean (4MM) averaged plots. Although 1-month SPEI was calculated for all datasets, we will only show results for 12-month SPEI

calculations due to the decreased variability tied to their longer calculation period. Any reference to SPEI in future sections is being made specifically to 12-month SPEI. Time series plots were not generated due to the discontinuous nature of the datasets.

Results and Discussion

Before comparing the first and last thirty year results for the ScenarioMIP models, it is first necessary to determine whether our initial SPEI calculations are reasonable. Plotted in Figure 2 are 12-month SPEI plots from the few overlapping years between ScenarioMIP simulations and SPEIDB calculations. While complete quantitative and spatial parity between models and observations is ultimately desired, in order to proceed we need only confirm that the models and our calculations produced reasonable SPEI values. The left column of data in Figure 2 reveals a consistency between individual model results (BCC) and the observed results (SPEIDB). Although, BCC depicts more extreme SPEI values, extending upwards of 2 in areas like the central Rocky Mountains of the United States and down to -2 in the Pacific northwest coast, these values' locations do vary massively from the SPEIDB results. Again, while spatially different in many places, similar extremes are reflected in SPEIDB, ranging closer to -2 to 1.5. The SPEI distributions of BCC and SPEIDB from June 2016 are plotted in Figure 3, where our visual analysis is confirmed by the similar, normal shape of both datasets, with BCC slightly preferring higher SPEI values around 2, while SPEIDB extends to 1.5. From this initial assessment we can conclude that our cal-

culations from the ScenarioMIP models reflect the appropriate distribution from observed values, and we may continue to interpret this modeled data.

Looking at the other figures in Figure 3, we notice an inversion of the trend from 2016 values when moving to the 2016-2021 averaged values. In these six year plots, we see an accumulation of high (around 1.5) SPEI in the Great Lakes region while the desert southwest accumulates a drying signal around -1. The model plot contrasts this with, BCC, showing a weakening signal, with extreme values pulling towards 0. There are many potential causes for this incongruity. The short, six year time frame of overlapping data is susceptible to the effects of shorter term variability such as the El Niño Southern Oscillation, and may cause issues for model outputs. Other recent socioeconomic phenomena, such as the COVID-19 pandemic, which caused a massive decrease in global CO_2 output in 2020 (Liu et al., 2020), may also contribute to model inconsistencies.

It is also important to draw attention to the effects of averaging different models over the same time period, evident as the four mean model (4MM) plots in Figure 3. Due to the large variability between model calculations, averaged plots across models have a tendency to "cancel out" one another, resulting in muted signals. Analysis following Figure 3 will attempt to mitigate this effect by adjusting plot colorbars to reflect more subtle SPEI fluctuations and by focusing on visual analysis to identify spatial modalities.

The averaged 2015-2044 June plots presented in Figure 4 depict a generally wet climate in the North American continent. Aside from the results of MRI, much of the continental United States is shown to have a slight but consistent average wetting trend across the first 30 years, best shown in the 4MM

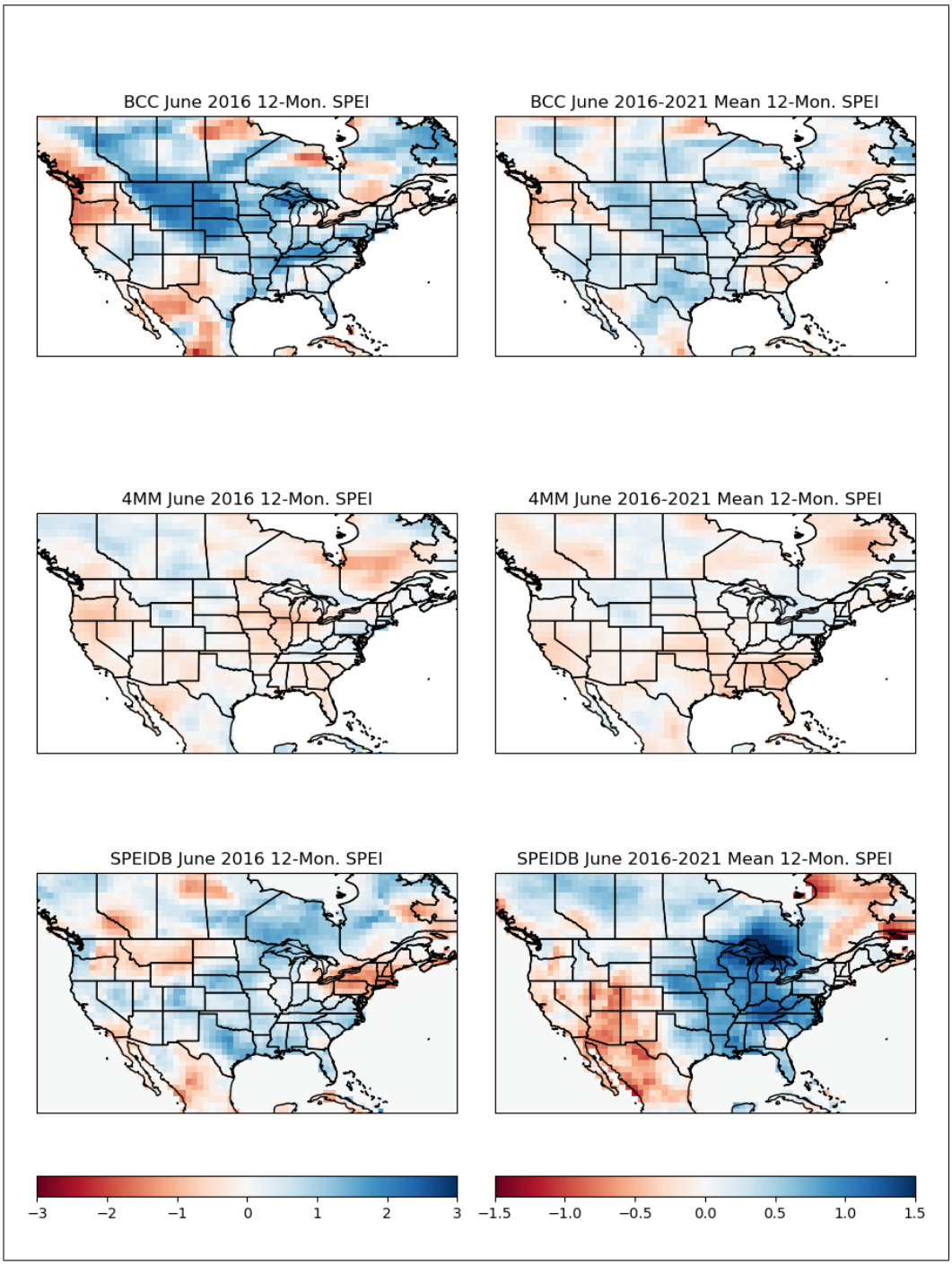

Figure 2: Plots of BCC, four model mean, and SPEI database 12-month SPEI calculations taken for June 2016 (left) and June 2016-2021 (right). Note the variation in colorbar scale from left to right columns due to the averaging of cell values over five years.

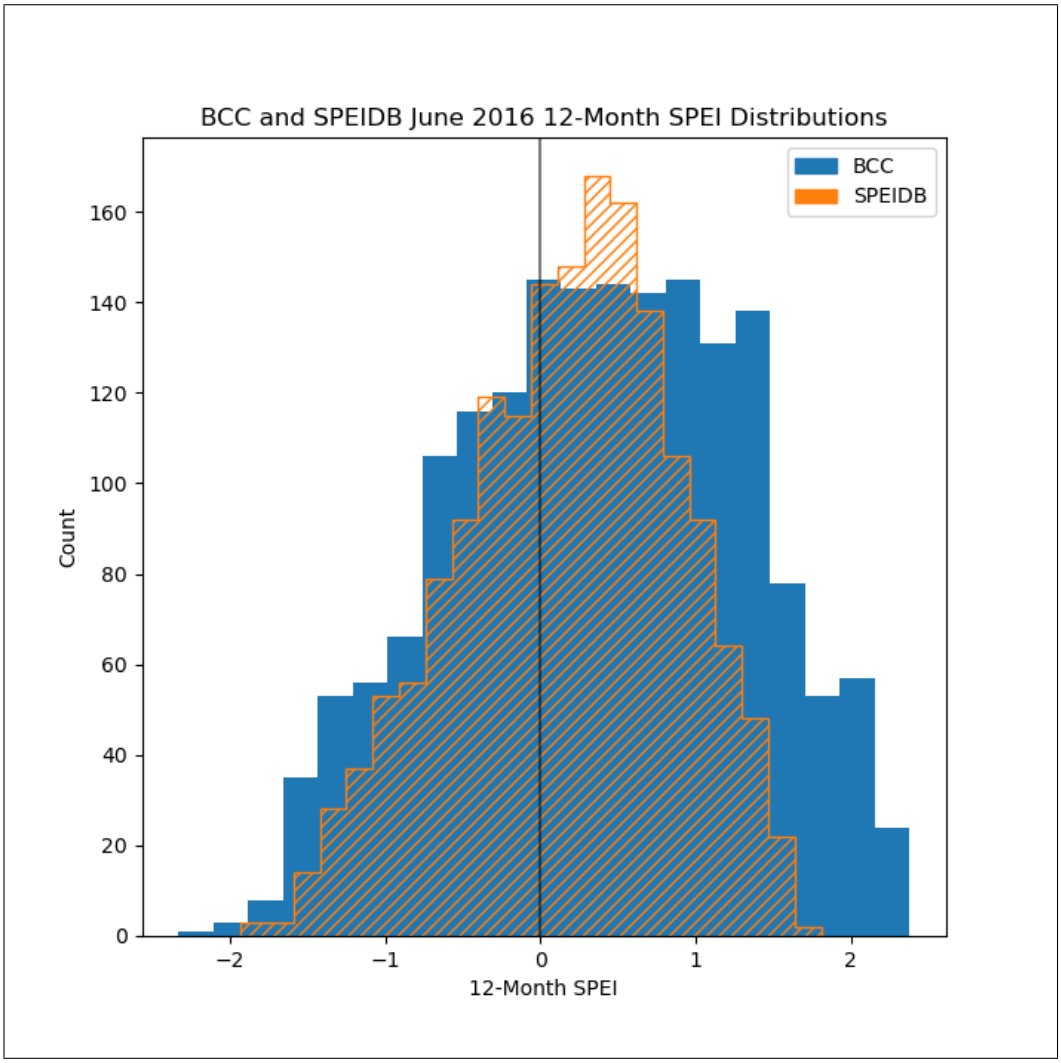

Figure 3: Overlayed histograms of BCC and SPEIDB 12-month SPEI values from cropped datasets. Histogram values are regridded to same 320×160 grid but are cropped to slightly different regions.

results with only sparse clusters of drying conditions in the desert southwest, the midwest, and along the Washington-Oregon border. While the drying trend along the Rocky Mountains in the MRI plot is not unprecedented in these models, the region is much wider in the east-west direction than what is shown in other models, such as BCC. For these first 30 year plots, we see no significant difference between the high and low ECS cases, CAN and MIROC respectively, with both models predicting slight drought conditions around the central midwest and generally wet conditions around California. MIROC, compared to CAN, predicts a wetter Montana, while extending the east-west trending drought signal from Utah to Missouri, a more extreme signal despite the model's significantly lower ECS value. While generally consistent with values from BCC and MIROC, CAN displays a notably larger wet signal over California, Nevada, and Utah, likely due in part to the low resolution and therefore large pixel cell size of CAN. The Rocky Mountain region, extending roughly from western Montana to northern New Mexico and Arizona is quite inconsistent between models, expressed as approximately zero in the 4MM plot. The high resolution plots, BCC and MRI, show a fairly consistent dry to neutral trend across this zone, conflicting noticeably with the massive wetting trend occupying much of the western United States in CAN's plot. The Great Plains region east of the Central Rocky Mountains, occupied by Nebraska, North Dakota, and South Dakota is another area of relatively high variability. BCC and CAN predict neutral SPEI values for this region, while MIROC predicts wetting in North Dakota and MRI models a drying South Dakota. These neutral and somewhat opposing plots average to a neutral or slightly wet region in the 4MM plot.

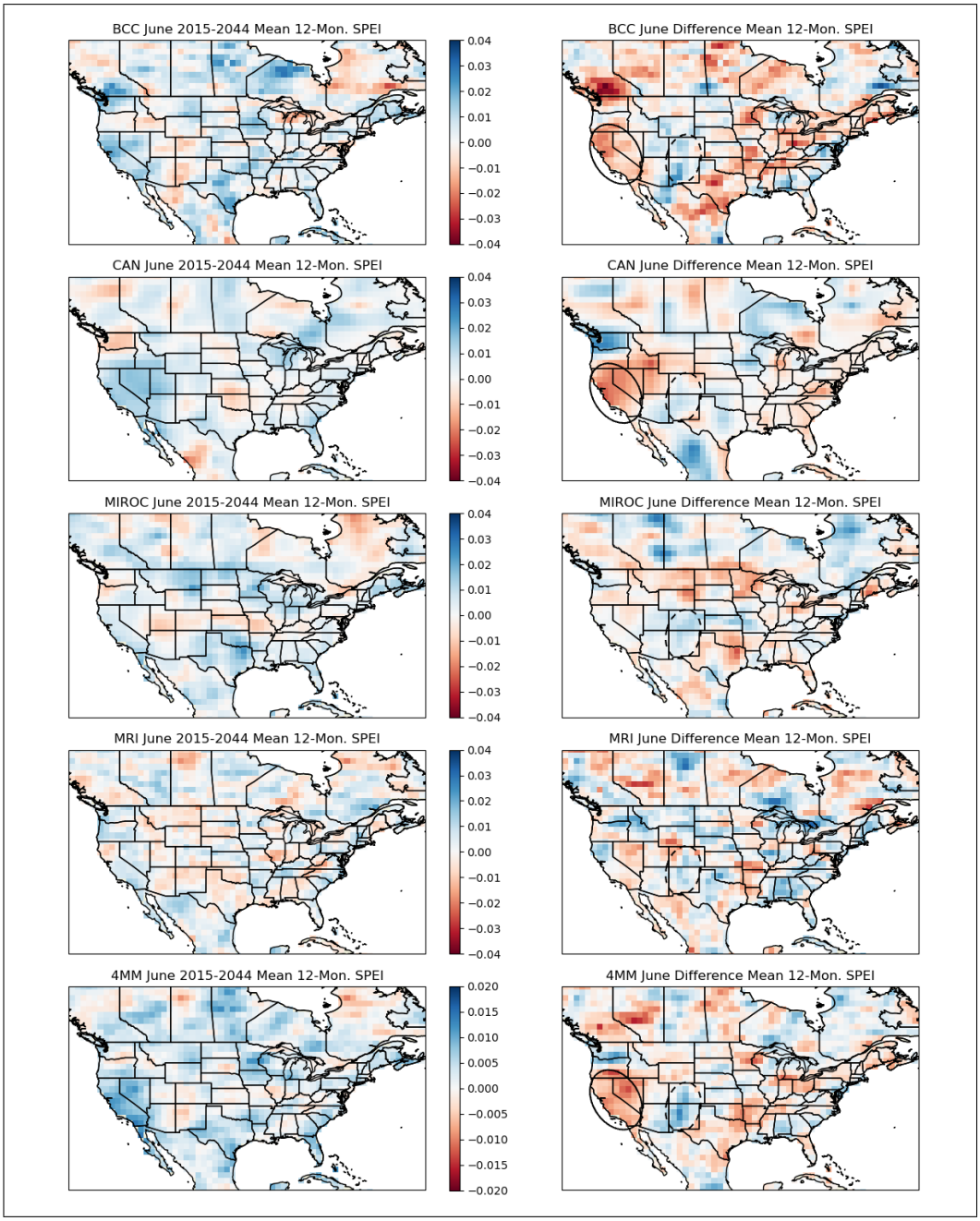

Figure 4: Plots of all four models and four model mean 12-month SPEI calculations taken from June 2015-2044 and the difference of June 2071-2100 subtracted by June 2015-2044. Colorbar scale shared across rows. Note two areas emphasized with solid and dotted ellipses in difference plots, only present where SPEI trends most visible.

While discussing specific magnitudes of SPEI and drawing predictions from these values is outside the scope of this study, it is important to note that the difference plots in Figure 4 are populated by more extreme values, an artifact of the subtraction, generating the difference plots and indicating significant changes in average June drought conditions. Two regions have been emphasized on the difference plots to aide description and will be referred to as the solid and dotted regions. The first of the two most conclusive regions in the difference plot highlights California, Nevada, and southern Oregon, or the solid region. This region highlights the most extreme and widespread drying across the entire study area, with clear drying occurring in 2 out of 4 models. MIROC calculations produced a neutral to slightly drying result while MRI had a still majority drying in Nevada with a notable cluster of wetting in northern California. While there is not total agreement between models, this is some of the strongest correlation seen in these plots, forecasting relatively severe drying trend through 2100.

The dotted region covers Colorado and New Mexico, encircling a consistent wetting trend between all models. While values vary slightly between models with BCC predicting a more extreme wetting in southwestern New Mexico, all four models agree that this region should expect a moderate wetting trend. This region may extend into Utah and Arizona, as shown in BCC and CAN, however results are less conclusive in these states. While a thorough discussion is outside the scope of this work, potentially interesting questions lie at the intersection of this wetting trend and the North American Monsoon, whose boundary closely matches our dotted region.

Results remain highly variable in the central United States, with this

agriculturally and economically significant area remaining highly inconclusive. BCC and MIROC show conflicting results for Kansas and Missouri, with the former predicting drying, especially in Missouri, while the latter predicts a moderate wetting trend for both states. Northern central states such as the Dakotas and Minnesota are predicted to be much dryer in MIROC simulations while slightly wetter in CAN and MRI simulations, producing fairly inconclusive results.

When considering resolution and ECS once more, we see no clear trend between the prediction tendencies of high and low ECS models when comparing CAN and MIROC respectively. This visual observation is confirmed in Figure 5, in which the histograms of CAN and MIROC cell values plot similarly. There is no significant trend for either model to prefer more extreme values or to skew to higher or lower values.

While many subregions within the United States remain confounding, this study has reinforced the IPCC's Sixth Annual Report and its findings that western North America will predominantly experience increased drought conditions (Pörtner et al., 2022). We have added greater specificity to the future drought trends within the western region, distinguishing a drying California-Nevada region and a wetting New Mexico-Colorado region.

Future studies investigating these regions should focus on the midwestern United States, adding more models and employing a variety of drought statistics to better understand model performance. These studies may not prove reliable until global ScenarioMIP models are run at higher resolutions, a factor that appeared to clarify our results despite not being thoroughly unpacked in this discussion.

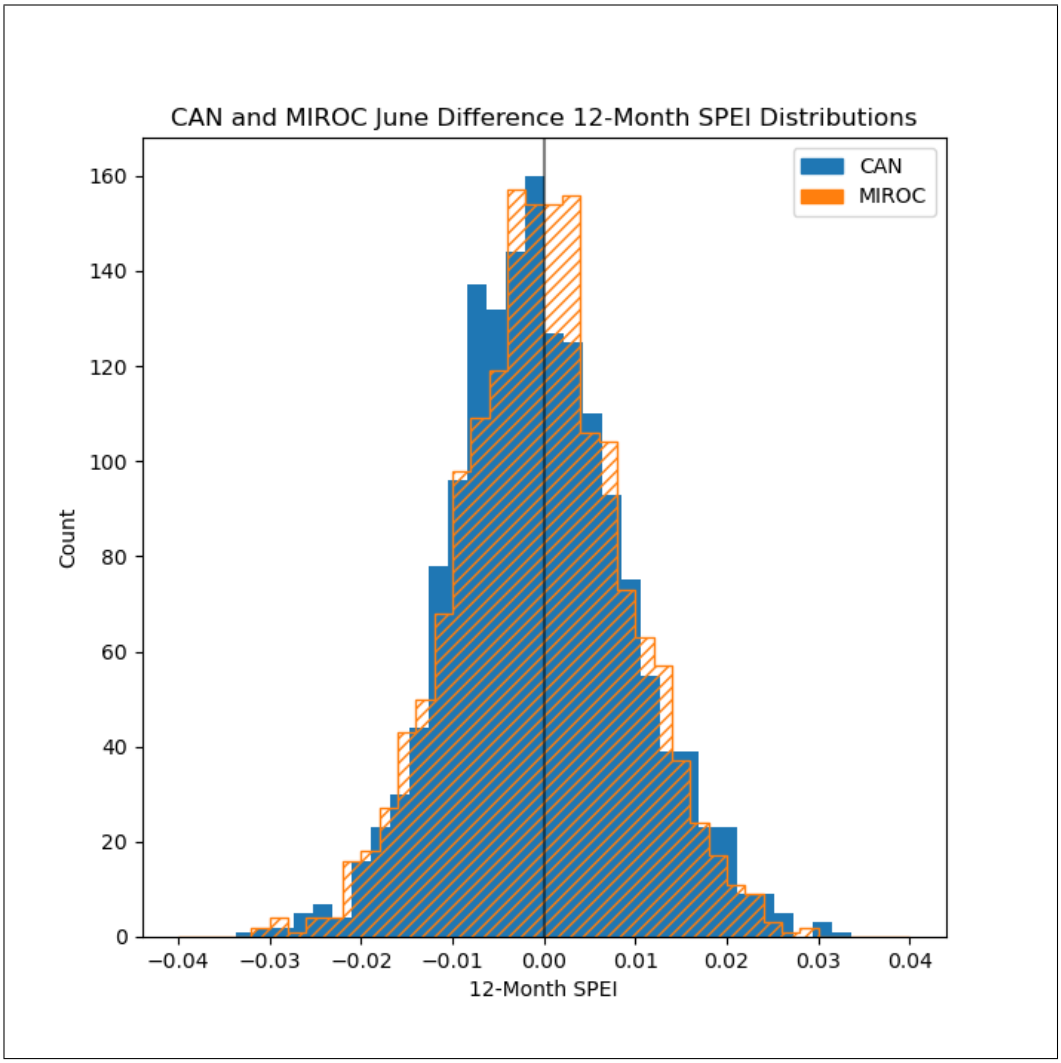

Figure 5: Overlayed histograms of CAN and MIROC (high and low ECS) 12-month SPEI values from cropped datasets.

References

Allen, R. G., Pereira, L. S., Raes, D., Smith, M., et al. (1998). Crop evapotranspiration-guidelines for computing crop water requirements-fao irrigation and drainage paper 56. *FAO, Rome*, *300*(9), D05109.

Basara, J. B., Maybourn, J. N., Peirano, C. M., Tate, J. E., Brown, P. J., Hoey, J. D., & Smith, B. R. (2013). Drought and associated impacts in the great plains of the united states—a review. *International Journal of Geosciences*, *04*(6), 72–81. https://doi.org/10.4236/ijg.2013.46A2009

Beguería, S., Vicente-Serrano, S. M., Reig, F., & Latorre, B. (2014). Standardized precipitation evapotranspiration index (spei) revisited: Parameter fitting, evapotranspiration models, tools, datasets and drought monitoring. *International journal of climatology*, *34*(10), 3001–3023.

Chen, D., Gao, G., Xu, C.-Y., Guo, J., & Ren, G. (2005). Comparison of the thornthwaite method and pan data with the standard penman-monteith estimates of reference evapotranspiration in china. *Climate research*, *28*(2), 123–132.

Cook, B. I., Smerdon, J. E., Seager, R., & Coats, S. (2014). Global warming and 21st century drying. *Climate Dynamics*, *43*(9), 2607–2627. https://doi.org/10.1007/s00382-014-2075-y

IPCC. (2022). Summary for policymakers [In Press]. In H. O. Pörtner, D. C. Roberts, M. Tignor, E. S. Poloczanska, K. Mintenbeck, A. Alegría, M. Craig, S. Langsdorf, S. Löschke, V. Möller, A. Okem, & B. Rama (Eds.), *Climate change 2022: Impacts, adaptation, and vulnerability. contribution of working group ii to the sixth assessment report of the intergovernmental panel on climate change* (In Press). Cambridge University Press.

Knutson, T. R., McBride, J. L., Chan, J., Emanuel, K., Holland, G., Landsea, C., Held, I., Kossin, J. P., Srivastava, A. K., & Sugi, M. (2010). Tropical cyclones and climate change. *Nature Geoscience*, *3*(3), 157–163. https://doi.org/10.1038/ngeo779

Liu, Z., Ciais, P., Deng, Z., Lei, R., Davis, S. J., Feng, S., Zheng, B., Cui, D., Dou, X., Zhu, B., et al. (2020). Near-real-time monitoring of global co2 emissions reveals the effects of the covid-19 pandemic. *Nature communications*, *11*(1), 5172.

McMichael, A. J., Woodruff, R. E., & Hales, S. (2006). Climate change and human health: Present and future risks. *The Lancet*, *367*(9513), 859–869. https://doi.org/10.1016/S0140-6736(06)68079-3

O'Neill, B. C., Kriegler, E., Ebi, K. L., Kemp-Benedict, E., Riahi, K., Rothman, D. S., Van Ruijven, B. J., Van Vuuren, D. P., Birkmann, J.,

Kok, K., et al. (2017). The roads ahead: Narratives for shared socioeconomic pathways describing world futures in the 21st century. *Global environmental change*, *42*, 169–180.

O'Neill, B. C., Tebaldi, C., van Vuuren, D. P., Eyring, V., Friedlingstein, P., Hurtt, G., Knutti, R., Kriegler, E., Lamarque, J.-F., Lowe, J., Meehl, G. A., Moss, R., Riahi, K., & Sanderson, B. M. (2016). The scenario model intercomparison project (ScenarioMIP) for CMIP6. *Geoscientific Model Development*, *9*(9), 3461–3482. https://doi.org/10.5194/gmd-9-3461-2016

Pan, S., Tian, H., Dangal, S. R., Yang, Q., Yang, J., Lu, C., Tao, B., Ren, W., & Ouyang, Z. (2015). Responses of global terrestrial evapotranspiration to climate change and increasing atmospheric co2 in the 21st century. *Earth's Future*, *3*(1), 15–35.

Panu, U. S., & Sharma, T. C. (2002). Challenges in drought research: Some perspectives and future directions. *Hydrological Sciences Journal*, *47*, S19–S30. https://doi.org/10.1080/02626660209493019

Pasteris, P., Svoboda, M., Redmond, K., Hayes, M., & Le Comte, D. (2005, March 22). Drought monitoring: New tools for the 21st century [Series Title: Books in Soils, Plants, and the Environment]. In D. Wilhite (Ed.), *Drought and water crises* (pp. 53–69, Vol. 107). CRC Press. https://doi.org/10.1201/9781420028386.ch3

Patz, J. A., Burke, T. A., & Balbus, J. M. (1996). Global climate change and emerging infectious diseases.

Pereira, L. S., Allen, R. G., Smith, M., & Raes, D. (2015). Crop evapotranspiration estimation with fao56: Past and future. *Agricultural Water Management*, *147*, 4–20.

Pörtner, H.-O., Roberts, D., Adams, H., Adelekan, I., Adler, C., Adrian, R., Aldunce, P., Ali, E., Begum, R. A., Friedl, B. B., Kerr, R. B., Biesbroek, R., Birkmann, J., Bowen, K., Caretta, M., Carnicer, J., Castellanos, E., Cheong, T., Chow, W., ... Ibrahim, Z. Z. (2022). *Climate change 2022: Impacts, adaptation and vulnerability*. Cambridge University Press.

Prein, A. F., Liu, C., Ikeda, K., Trier, S. B., Rasmussen, R. M., Holland, G. J., & Clark, M. P. (2017). Increased rainfall volume from future convective storms in the us. *Nature Climate Change*, *7*(12), 880–884.

Ruhe, L. (2022). A comparison of drought indices in CMIP6 climate projections.

Sentelhas, P. C., Gillespie, T. J., & Santos, E. A. (2010). Evaluation of fao penman–monteith and alternative methods for estimating reference evapotranspiration with missing data in southern ontario, canada. *Agricultural water management*, *97*(5), 635–644.

Shiogama, H., Abe, M., & Tatebe, H. (2019). Miroc miroc6 model output prepared for cmip6 scenariomip ssp245. https://doi.org/10.22033/ESGF/CMIP6.5746

Stevens-Rumann, C. S., Kemp, K. B., Higuera, P. E., Harvey, B. J., Rother, M. T., Donato, D. C., Morgan, P., & Veblen, T. T. (2018). Evidence for declining forest resilience to wildfires under climate change (F. Lloret, Ed.). *Ecology Letters*, *21*(2), 243–252. https://doi.org/10.1111/ele.12889

Swart, N. C., Cole, J. N., Kharin, V. V., Lazare, M., Scinocca, J. F., Gillett, N. P., Anstey, J., Arora, V., Christian, J. R., Jiao, Y., Lee, W. G., Majaess, F., Saenko, O. A., Seiler, C., Seinen, C., Shao, A., Solheim, L., von Salzen, K., Yang, D., ... Sigmond, M. (2019). Cccma canesm5 model output prepared for cmip6 scenariomip ssp245. https://doi.org/10.22033/ESGF/CMIP6.3685

Vicente-Serrano, S. M., Beguería, S., & López-Moreno, J. I. (2010). A multiscalar drought index sensitive to global warming: The standardized precipitation evapotranspiration index. *Journal of climate*, *23*(7), 1696–1718.

Vicente-Serrano, S. M., Beguería, S., Lorenzo-Lacruz, J., Camarero, J. J., López-Moreno, J. I., Azorin-Molina, C., Revuelto, J., Morán-Tejeda, E., & Sanchez-Lorenzo, A. (2012). Performance of drought indices for ecological, agricultural, and hydrological applications. *Earth Interactions*, *16*(10), 1–27.

Wan, W., Zhao, J., Popat, E., Herbert, C., & Döll, P. (2021). Analyzing the impact of streamflow drought on hydroelectricity production: A global-scale study. *Water Resources Research*, *57*(4). https://doi.org/10.1029/2020WR028087

Xin, X., Wu, T., Shi, X., Zhang, F., Li, J., Chu, M., Liu, Q., Yan, J., Ma, Q., & Wei, M. (2019). Bcc bcc-csm2mr model output prepared for cmip6 scenariomip ssp245. https://doi.org/10.22033/ESGF/CMIP6.3030

Yukimoto, S., Koshiro, T., Kawai, H., Oshima, N., Yoshida, K., Urakawa, S., Tsujino, H., Deushi, M., Tanaka, T., Hosaka, M., Yoshimura, H., Shindo, E., Mizuta, R., Ishii, M., Obata, A., & Adachi, Y. (2019). Mri mri-esm2.0 model output prepared for cmip6 scenariomip ssp245. https://doi.org/10.22033/ESGF/CMIP6.6910

Zelinka, M. D., Myers, T. A., McCoy, D. T., Po-Chedley, S., Caldwell, P. M., Ceppi, P., Klein, S. A., & Taylor, K. E. (2020). Causes of higher climate sensitivity in cmip6 models. *Geophysical Research Letters*, *47*(1).